



Development of a Novel Electron Cyclotron Resonance Magnetic Nozzle Thruster with Magnetically Thickened Resonance Region

Hitchens, Oliver; Lucca Fabris, Andrea

[https://openresearch.surrey.ac.uk/esploro/outputs/conferenceProceeding/Development-of-a-Novel-Electron-Cyclotron/99991466502346/filesAndLinks
?index=0](https://openresearch.surrey.ac.uk/esploro/outputs/conferenceProceeding/Development-of-a-Novel-Electron-Cyclotron/99991466502346/filesAndLinks?index=0)

Hitchens, O., & Lucca Fabris, A. (2025). Development of a Novel Electron Cyclotron Resonance Magnetic Nozzle Thruster with Magnetically Thickened Resonance Region. <https://doi.org/>

Development of a Novel Electron Cyclotron Resonance Magnetic Nozzle Thruster with Magnetically Thickened Resonance Region

IEPC-2024-157

*Presented at the 38th International Electric Propulsion Conference, Toulouse, France
June 23-28, 2024*

Oliver Hitchens* and Andrea Lucca Fabris†
University of Surrey, Guildford, GU2 7XH, United Kingdom

An electron cyclotron resonance (ECR) magnetic nozzle plasma thruster typically consists of a microwave antenna and a magnetic nozzle. The magnetic field forms a region where the propellant is resonantly heated and ionised by the microwaves. The ionised gas is then accelerated out of the magnetic nozzle, generating thrust. The design of these thrusters to date has not accounted for the thickness of the resonance region, often assuming it to be near zero. Two test campaigns have been conducted in which the thickness of the resonance region was varied. Larger resonance region thicknesses are seen to increase thrust and specific impulse by up to 60 % and thrust efficiency by up to 32 %. Experimental measurements of electron temperature, plasma potential and ion current indicate that increased electron heating in the larger resonance volume leads to a stronger electrostatic field and higher ion beam current. This study presents strong evidence that optimising for a thickened resonance region can significantly enhance thruster performance.

Nomenclature

Δx_D	= resonance region thickness due to doppler broadening [m]
$\frac{\partial B}{\partial x}$	= magnetic field strength gradient [T/m]
$v_{ }$	= electron mean axial velocity [m/s]
B_0	= magnetic field strength at resonance [T]
B_{Dl}	= lower bound of the doppler broadened resonance region [T]
B_{Du}	= upper bound of the doppler broadened resonance region [T]
e	= elementary charge [C]
f_c	= electron cyclotron frequency [Hz]
f_m	= driving microwave frequency [Hz]
m_e	= mass of an electron [kg]

*PhD Candidate, Surrey Space Centre, o.hitchens@surrey.ac.uk

†Senior Lecturer, Surrey Space Centre, a.luccafabris@surrey.ac.uk

I. Introduction to ECR Magnetic Nozzle Thrusters

ELECTRON cyclotron resonance (ECR) magnetic nozzle plasma thrusters typically comprise a central chamber, microwave antenna and magnetic nozzle, see figure 1. Gaseous propellant is injected into the central chamber where it is ionised by microwave radiation emitted by the antenna. A magnetic nozzle accelerates the electrons out of the thruster, this generates a negative charge downstream that acts to accelerate the positive ions towards the electrons, out of the thruster, generating thrust. The acceleration of ions due to this charge separation is known as ambipolar acceleration.

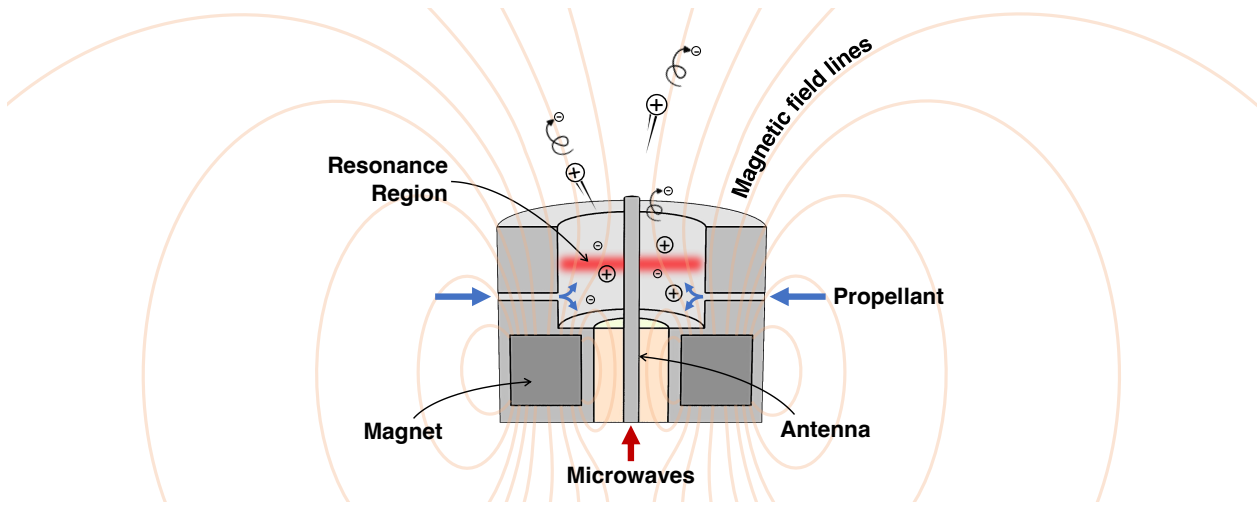


Figure 1: Simplified cross-sectional diagram of a coaxial ECR magnetic nozzle thruster.

The performance of an ECR thruster is highly dependant on the heating of electrons by microwave radiation. This heating predominantly occurs in the resonance region, see figure 1, where the rotational frequency of the electrons around magnetic field lines matches the microwave frequency. The electron cyclotron frequency is dependant solely on the local magnetic field strength. Therefore, for a given microwave frequency, the location of the resonance region within the central chamber is defined by this local magnetic field strength, see equation 1.¹

$$B_0 = \frac{2\pi m_e f_m}{e} \quad (1)$$

Where B_0 is the magnetic field strength at resonance in tesla at which the electrons are resonantly heated by the microwaves, m_e is the mass of an electron in kilograms, f_m is the driving microwave frequency in hertz and e is the elementary charge in coulombs.

II. How to Magnetically Thicken the Resonance Region

Equation 1 implies a thin resonance region, with thickness only being introduced by a range in the driving microwave frequency, f_m , due to the microwave signal's bandwidth. The solid state microwave generator used in this study has a -3 dB bandwidth of less than 0.1 MHz, resulting in a resonance region thickness of approximately 1 micrometer for the thrusters outlined in this paper.

Electrons accelerated downstream by the magnetic nozzle experience an electrostatic force pulling them back towards the thruster. Electrons that are pulled back upstream are reflected by a magnetic mirror located at the rear of the thruster chamber. Electrons that are trapped between this magnetic mirror and the electrostatic field gain further energy from the microwaves, accelerating them to high velocities. The high velocity electrons experience a doppler shifted driving microwave frequency, which changes the magnetic field strength at which they are resonantly heated. The large range of electron velocities has the effect of broadening the resonance region. The thickness of the resonance region due to doppler broadening can be calculated using equation 2.²

$$\Delta x_D = \sqrt{\frac{\nu_{\parallel}}{\frac{f_c}{B_0} |\frac{\partial B}{\partial x}|}} \quad (2)$$

Where Δx_D is the resonance region thickness due to doppler broadening in meters, ν_{\parallel} is the electrons mean axial velocity in meters per second, f_c is the electron cyclotron frequency in hertz, B_0 is the magnetic field strength at resonance in tesla and $|\frac{\partial B}{\partial x}|$ is the gradient of the magnetic field in tesla per meter. A particle in cell simulation developed by Porto et al.³ shows electrons gaining energy in a region approximately 4 mm before and 4 mm after the resonance region. This provides strong evidence for the existence of a doppler broadened resonance region.

By decreasing the magnetic field strength gradient at resonance, $\frac{\partial B}{\partial x}$, the resonance region thickness, Δx_D , can be increased, see equation 2. This is the driving principle behind both studies outlined in this paper.

III. Electromagnetically Thickening the Resonance Region

A. Thruster Design

The design of the thruster used in this study has been informed from work conducted by ONERA.⁴ A diagram of the thruster is shown in figure 2, with photos of it operating without its electromagnetic coil shown in figure 3. Testing was conducted in a cylindrical vacuum chamber 3.0 m in length and 1.8 m in diameter. One turbomolecular pump, one cryopump and one 660 mm diameter cryopanel were used to maintain background pressure during tests. ECR thruster performance is found to increase significantly at lower background pressures and larger facility sizes.⁵ The experimental measurements of performance reported in this paper are therefore lower than the expected in-space performance of these thrusters.

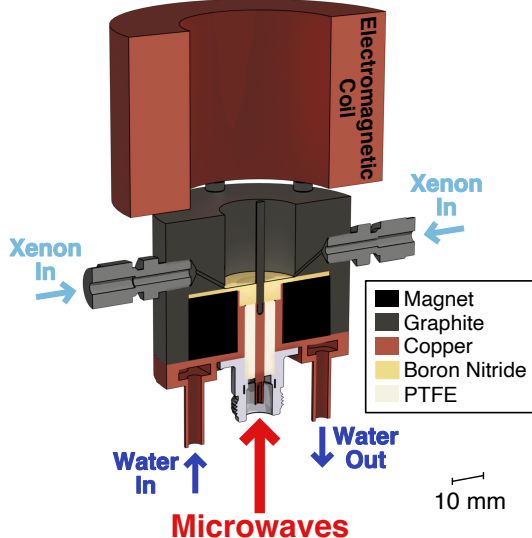


Figure 2: Cross-sectional view of the electromagnetic thruster under test.

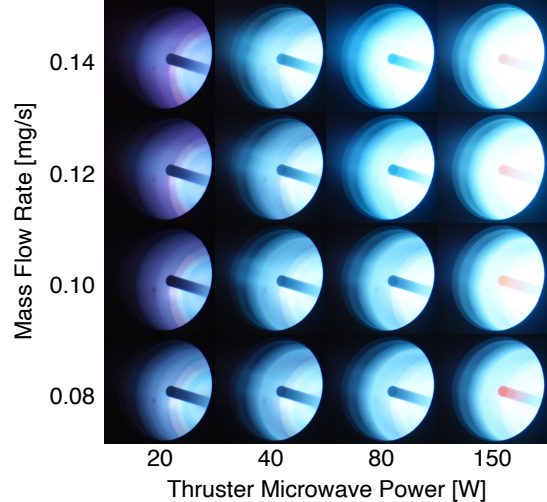


Figure 3: Photos of the thruster operating at different powers and xenon mass flow rates at a backing pressure of 6.8×10^{-6} mbar. Electromagnetic coil was removed to enable visibility of the antenna.

An axisymmetric magnetic field model of the thruster was created using Finite Element Method Magnetics.⁶ By sweeping the current through the electromagnetic coil, the magnetic field gradient at resonance can be varied, see figure 4. This allows for the calculation of resonance region thickness, Δx_D , using equation 2. This assumes the same axial electron velocity as Porto et al. of 3.0×10^6 m/s.³ The resonance region thickness can be seen to be greatest at 3 amps of coil current, see table 1.

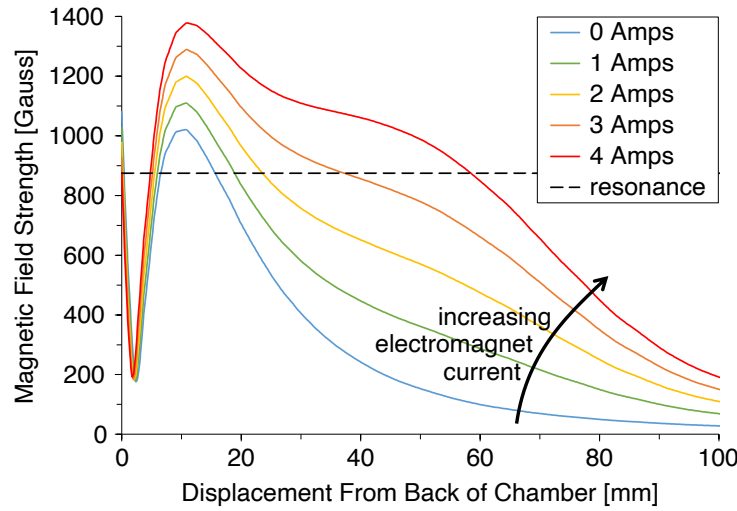


Figure 4: Magnetic field strength plot for varying coil currents. Each solid line shows the change in magnetic field strength with respect to displacement from the back of the thrusters chamber along its central axis. Data was obtained from the same model shown in figure 5. The dashed line shows the magnetic field strength at which resonance occurs, 875 Gauss.

coil current	0 A	1 A	2 A	3 A	4 A
$ \frac{\partial B}{\partial x} $ [T/m]	3.82	3.69	2.31	0.69	1.66
Δx_D [mm]	5.30	5.39	6.81	12.46	8.04
B_{Dl} [Gauss]	774	776	796	832	808
B_{Du} [Gauss]	976	974	954	918	942

Table 1: Values that define the doppler broadened resonance region along the central axis for each electromagnetic coil current.

As the rate of change of magnetic field strength gradient is relatively small, we can make the assumption that magnetic field strength gradient remains constant within the resonance region. This allows for the calculation of the lower and upper bounds of the doppler broadened resonance regions, see equations 3 and 4.

$$B_{Dl} = B_0 - \left| \frac{\partial B}{\partial x} \right| \frac{\Delta x_D}{2} \quad (3)$$

$$B_{Du} = B_0 + \left| \frac{\partial B}{\partial x} \right| \frac{\Delta x_D}{2} \quad (4)$$

Where B_{Dl} and B_{Du} are the lower and upper bounds of the doppler broadened resonance region in tesla, B_0 is the magnetic field strength at resonance in Tesla, $\left| \frac{\partial B}{\partial x} \right|$ is the gradient of the magnetic field in tesla per meter and Δx_D is the resonance region thickness due to doppler broadening in meters.

The size of the doppler broadened resonance region can be visualised as the region between the lower and upper bounds of the doppler broadened resonance regions, B_{Dl} and B_{Du} . This is shown as the red regions in figure 5. This assumes that there is a negligible change in magnetic field strength gradient with radial displacement. Further work should aim to define the resonance region across the radius of the thruster, to increase the accuracy of this model.

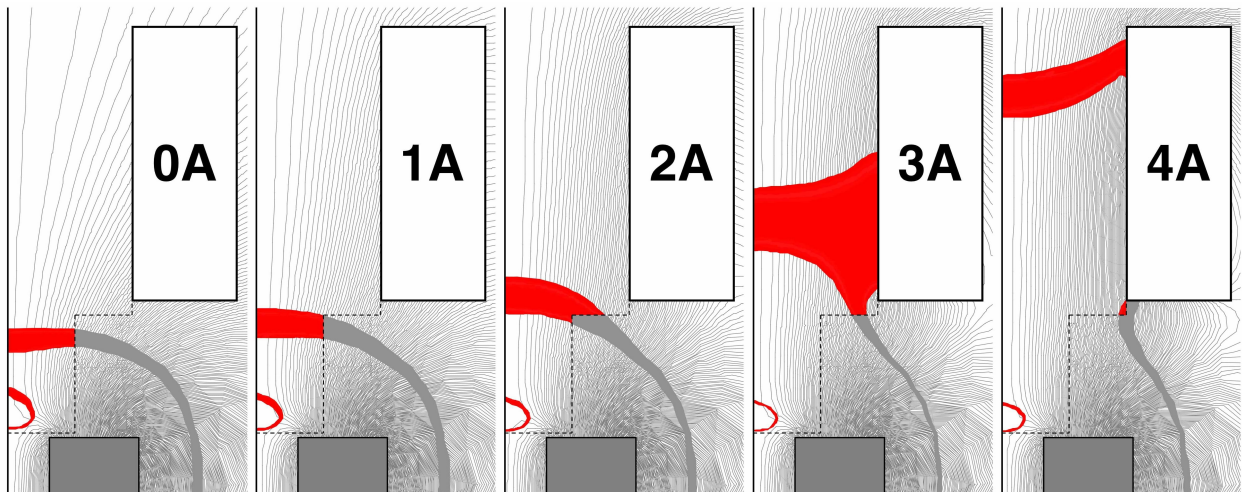


Figure 5: Axisymmetric magnetic field model of the thruster with a permanent magnet upstream of the chamber and an electromagnet downstream of the chamber. The model is run with varying currents through the coil, from 0 amps to 4 amps. The grey box shows the permanent magnet, the white box shows the electromagnet and the dashed lines outline the chamber boundary. The resonance region is defined as the region between B_{Dl} and B_{Du} and is shown in red when inside the chamber, or grey when outside the chamber.

B. Experimental Results

Direct thrust measurements were taken using a torsional thrust balance⁷ and are plotted in figure 6a. These are plotted alongside the normalised cross-sectional resonance area, which is simply the normalised area of the red regions in figure 5. Ion beam current has also been measured with a faraday probe and is plotted alongside normalised cross-sectional resonance area in figure 6b. Both thrust and ion beam current peak at 3 amps and show a strong correlation with cross-sectional resonance area. The fact that both thrust and ion beam current can be seen to decrease after 3 amps shows us that this performance increase is not due to the changing position of the resonance region or the changing divergence of the magnetic field. This leaves only the enlarged resonance region as the cause for the increased performance.

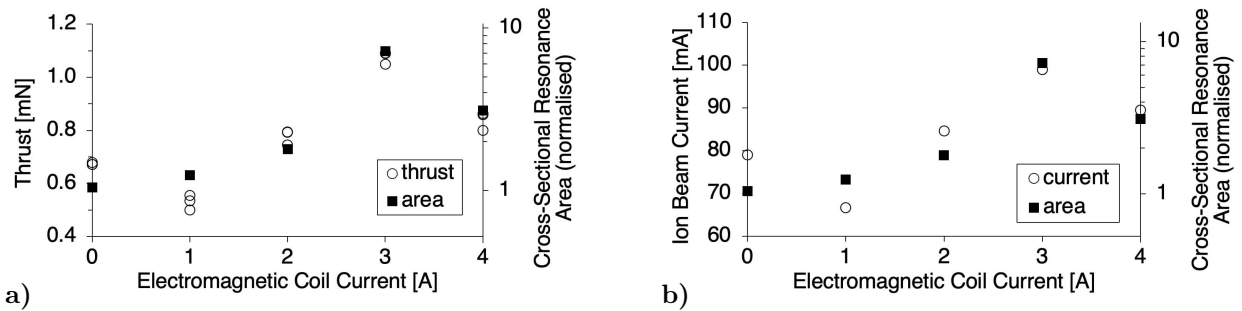


Figure 6: a) Thrust and cross-sectional resonance area (normalised) over electromagnetic coil current. b) Ion beam current and cross-sectional resonance area (normalised) over electromagnetic coil current. The thruster was operated with 74 W thruster power and 0.10 mg/s xenon mass flow rate at a backing pressure of 6.8×10^{-6} mbar. Three thrust readings were taken for each coil current with a mean standard deviation of 0.023 mN. Cross-sectional resonance area is calculated from the red regions in figure 5.

Langmuir probe measurements of electron temperature and plasma potential, taken 49 mm downstream of the electromagnets, are shown in figure 7.⁸ Electron temperature can be seen to peak at 3 amps of coil current, suggesting that the larger resonance region is increasing electron heating. The increased electron thermal energy produces a stronger ambipolar electric field, as shown in figure 7b. This increases the kinetic energy of the ions, leading to the increase in thrust and ion beam current shown in figure 6.

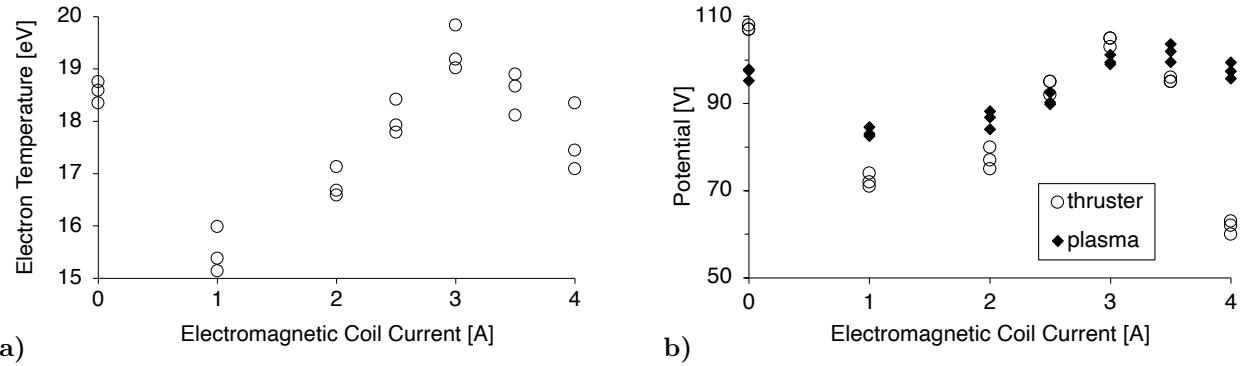


Figure 7: **a)** Electron temperature over electromagnetic coil current. **b)** Thruster floating potential and plasma potential over electromagnetic coil current. The thruster was operated with 69 W thruster power and 0.10 mg/s xenon mass flow rate at a backing pressure of 6.5×10^{-6} mbar. Three of each measurement was taken for each coil current. Electron temperature measurements have a mean standard deviation of 0.39 eV. Thruster potential measurements have a mean standard deviation of 1.37 V. Plasma potential measurements have a mean standard deviation of 1.58 V.

Increasing the volume of the resonance region has increased both thrust and specific impulse by 60 %, see figure 6a. Thruster efficiency is increased by 16 %, or 174 % if the power to the electromagnet is ignored. This study therefore presents strong evidence that optimising for a thickened resonance region can significantly increase thruster performance.

IV. Ferromagnetically Thickening the Resonance Region

A. Thruster Design

A disadvantage of the thruster outlined in the previous section is it's power loss to the electromagnet, reducing total efficiency. In this section, passive thickening of the resonance region is explored using ferromagnetic material. A large ECR thruster is built, similar in size to ONERA's 200 W ECRA thruster.⁵ It comprises a central thrust chamber 72 mm in diameter and 20 mm deep, as well as a central antenna 2.5 mm in diameter and 20 mm long, see figures 9 and 8. Both are made from isostatic graphite. The addition of a iron ring immediately downstream of the permanent ring magnet decreases the magnetic field gradient at resonance, see figure 10. This has the effect of thickening the resonance region.

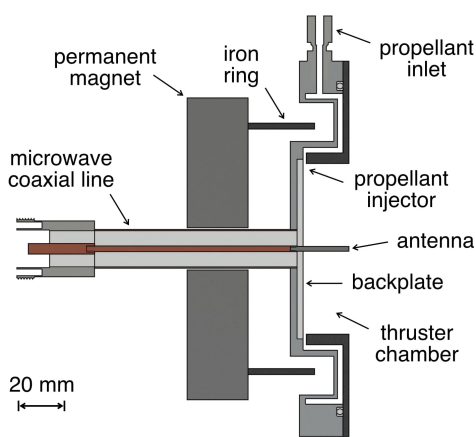


Figure 8: Labeled cross-sectional view of the thruster under test.

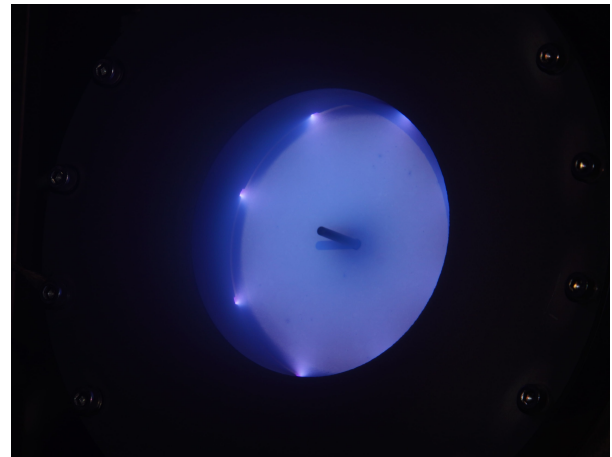


Figure 9: Photo of the thruster operating with 145 W thruster power and 0.39 mg/s xenon mass flow rate at a backing pressure of 5.3×10^{-6} mbar.

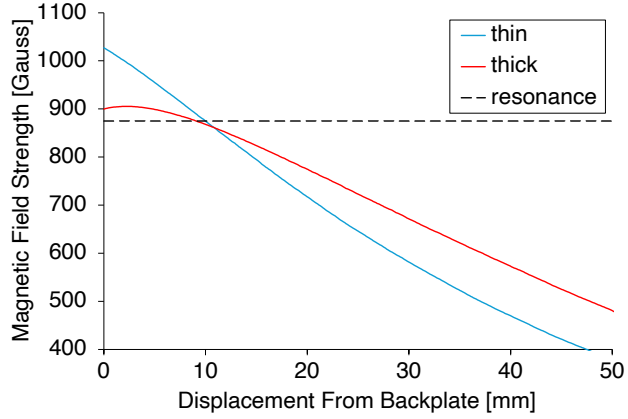


Figure 10: Magnetic field strength plot for the thruster without the iron ring (thin resonance region) and with the iron ring (thick resonance region). Solid lines show the change in magnetic field strength with respect to displacement from the backplate along the central axis. Data was obtained from the same model shown in figure 11. The dashed line shows the magnetic field strength at which resonance occurs, 875 Gauss.

Using equation 2 the doppler broadened resonance region thickness, Δx_D , can be calculated, see table 2. The upper and lower bounds of the doppler broadened resonance region are calculated using equations 3 and 4. The doppler broadened resonance region defined by these bounds is shown in figure 11

	Thin	Thick
$ \frac{\partial B}{\partial x} $ [T/m]	1.68	0.73
Δx_D [mm]	7.99	12.11
B_{Dl} [Gauss]	808	831
B_{Du} [Gauss]	942	919

Table 2: Values that define the doppler broadened resonance region along the central axis for the thruster without the iron ring (thin resonance region) and with the iron ring (thick resonance region).

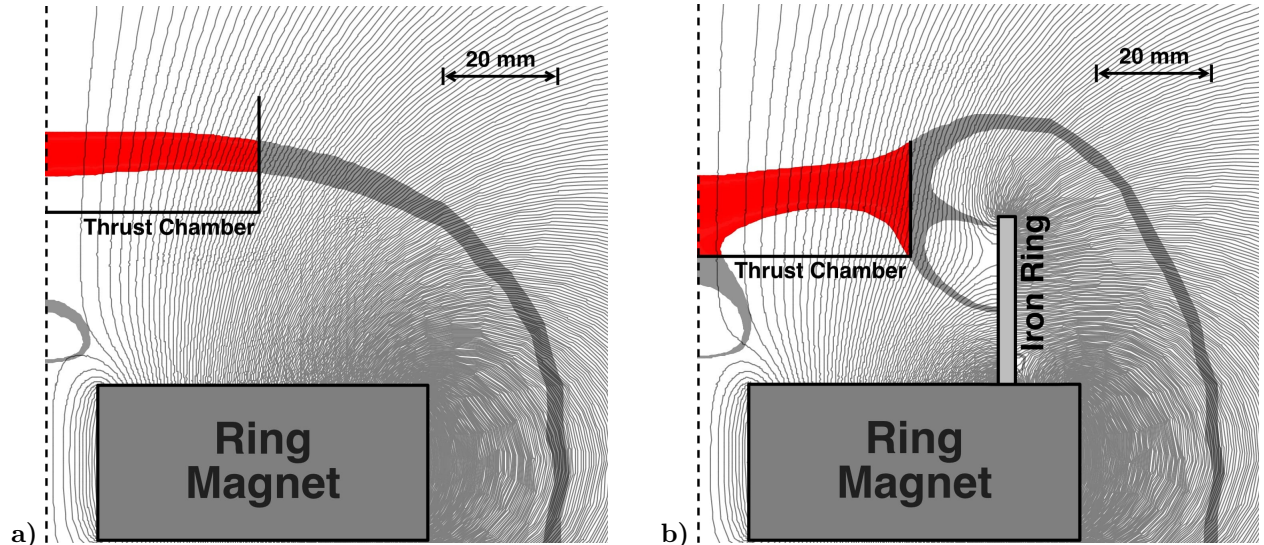


Figure 11: Axisymmetric magnetic field model. **a)** Thruster without iron ring (thin resonance region). **b)** Thruster with iron ring (thick resonance region). The portion of the resonance region that resides inside the thrust chamber is shown in red. Resonance region residing outside the thrust chamber shown in grey.

B. Experimental Results

Direct thrust measurements were taken over a range of mass flow rates and thruster powers, see figure 12. The thick resonance region can be seen to increase thrust for all mass flow rates and thruster powers tested. The larger resonance region also allows for the thruster to operate at a lower mass flow rate, see figure 12a. At 0.39 mg/s and 145 W, the addition of the iron ring can be seen to increase thrust and specific impulse by 15 % while thrust efficiency increases by 32 %.

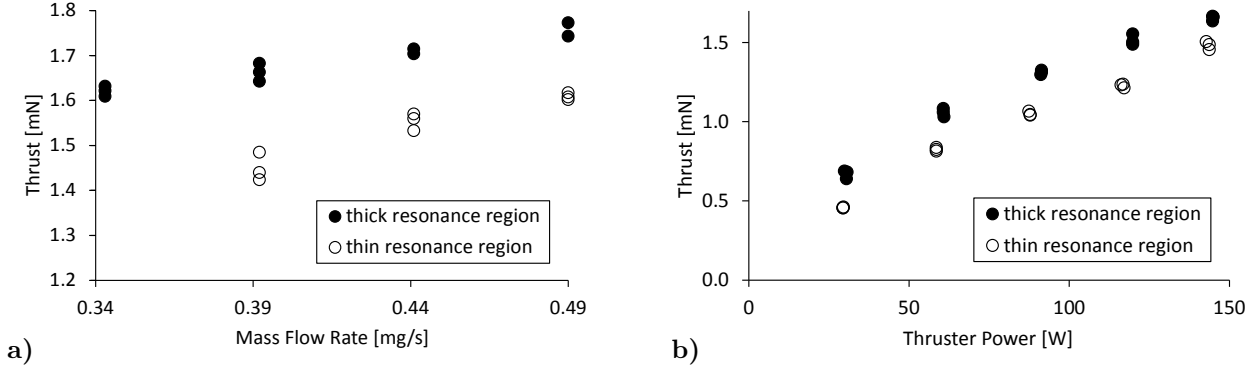


Figure 12: a) Thrust over xenon mass flow rate for both the thick and thin resonance region at 145 W thruster power. b) Thrust over thruster power for both the thick and thin resonance region at 0.39 mg/s xenon mass flow rate. Three readings were taken for each test condition with a mean standard deviation of 0.015 mN. Measurements were taken at a backing pressure of 5.3×10^{-6} mbar.

Testing was conducted in a cylindrical vacuum chamber 3.0 m in length and 1.8 m in diameter. One cryopump and one 660 mm diameter cryopanel were used to maintain backing pressure during tests.

The floating potential of the thruster is a strong indicator of thruster performance. This is because it is a measurement of the strength of the ambipolar electric field that is responsible for ion acceleration. Measurements of thruster floating potential were taken using a multimeter over a range of mass flow rates and thruster powers, see figure 13. A clear increase in thruster floating potential is seen for the thickened resonance region across all test conditions.

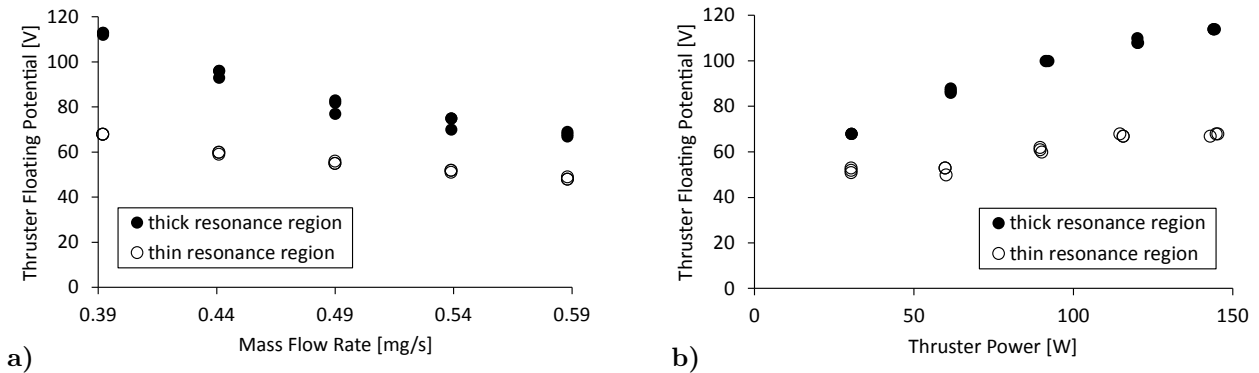


Figure 13: a) Thruster floating potential over mass flow rate for both the thick and the thin resonance region at 145 W thruster power. b) Thruster floating potential over thruster power for both the thick and the thin resonance region at 0.39 mg/s xenon mass flow rate. Three readings were taken for each test condition with a mean standard deviation of 0.77 V. Measurements were taken at a backing pressure of 7.1×10^{-6} mbar.

A faraday probe on a rotational stage was swept 110 degrees through the thrusters plume at a distance of 427 mm from the thruster. Measurements of ion current density for different thruster powers are shown in figure 14. At 143 W thruster power, thickening the resonance region is seen to decrease the far field divergence angle from 55° to 51° .⁹ However a decrease in the magnetic field divergence observed in figure 11 could also be responsible for this.

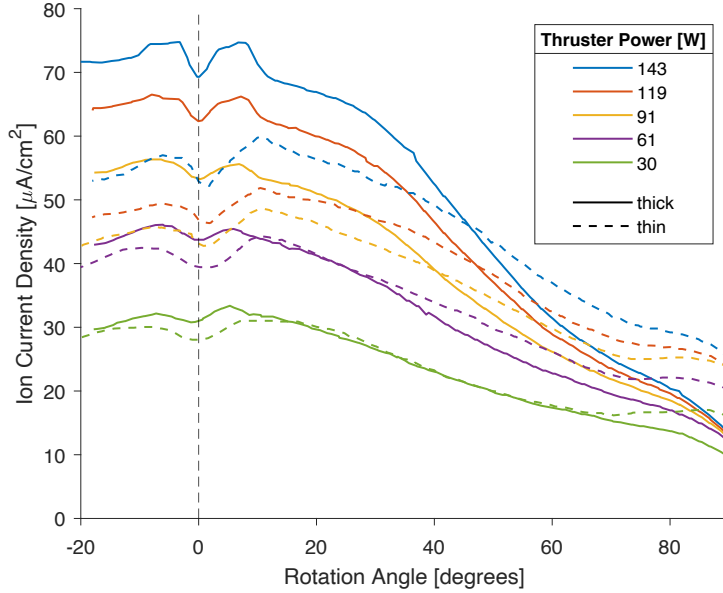


Figure 14: Ion current density over rotation angle for five different thruster powers. Thick resonance region shown as solid line, thin resonance region shown as dashed line. Where at 0 degrees the probe is aligned with the central axis of the thruster. -1.0 kV probe bias was required to repel the high energy electrons. The thruster was operated with 0.39 mg/s xenon mass flow rate at a backing pressure of 6.5×10^{-6} mbar.

C. Resonance Region Location

A translational stage attached to the base of the thruster allows for the chamber to be moved axially, while the magnetic assembly remains fixed. This allows for the location of the resonance region within the central chamber to be optimised for maximum performance.

Thrust is plotted against the downstream displacement of the thin resonance region from the backplate, see figure 15a. No measurements were recorded at 0 mm displacement, as the thruster was unable to maintain a plasma. The results shown in figure 15 were taken without the use of the iron ring to thicken the resonance region. A decrease in thrust is seen at displacements below 8 mm, indicating an interaction of the resonance region with the backplate.

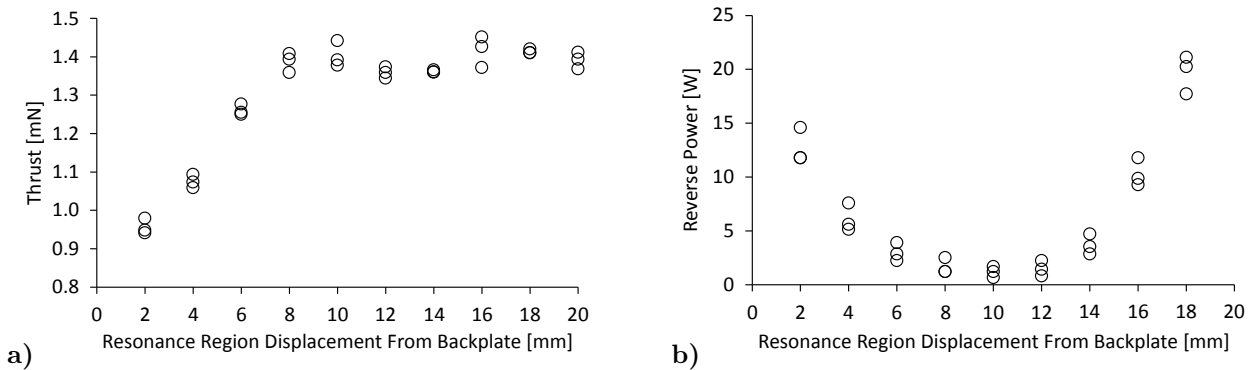


Figure 15: **a)** Thrust over the displacement of the resonance region from the backplate. **b)** Reverse microwave power over the displacement of the resonance region from the backplate. The thruster was operated with 143 W thruster power at displacements of 8 mm, 10 mm and 12 mm, powers at other displacements can be found by subtracting the corresponding reverse power. The thruster was operated with 0.39 mg/s xenon mass flow rate at a backing pressure of 6.5×10^{-6} mbar. Three measurements were taken for each test condition with mean standard deviations of 0.02 mN and 0.86 W respectively.

Reverse microwave power is plotted against the downstream displacement of the thin resonance region from the backplate, see figure 15b. As reverse power can be seen to be lowest at 10 mm displacement, this was the position of the resonance region that was chosen for all other tests. Similarly, when the resonance region is thickened with the iron ring, the optimum resonance region position was also found to reside at the centre of the thrust chamber.

V. Conclusion

Two different ECR magnetic nozzle thrusters have been developed and studied. The first has shown how a magnetically thickened resonance region can be formed using an electromagnet. A strong correlation has been found between the size of the resonance region and the performance of the thruster. By magnetically thickening the resonance region, thrust and specific impulse were increased by 60 %, while thruster efficiency was only increased by 16 % due to power losses in the electromagnet.

The second thruster aimed to further increase thruster efficiency by using an iron ring instead of an electromagnet to thicken the resonance region. This thruster only saw an increase in thrust and specific impulse of 15 % when the resonance region was magnetically thickened. However thruster efficiency was increased by 32 %, proving the efficacy of the design. A more detailed evaluation of both thrusters is planned, in two separate journal papers.

These studies therefore provide strong evidence that optimising for a thickened resonance region can significantly increase thruster performance.

References

- ¹Jarrige, J. et al., “Characterization of a coaxial ECR plasma thruster,” *44th AIAA Plasmadynamics and Lasers Conference*, 2013.
- ²Williamson, M. C., Lichtenberg, A. J., and Lieberman, M. A., “Self-consistent electron cyclotron resonance absorption in a plasma with varying parameters,” *Journal of Applied Physics*, Vol. 72, No. 9, 11 1992, pp. 3924–3933.
- ³Porto, J., Elias, P. Q., and Ciardi, A., “Anisotropic electron heating in an electron cyclotron resonance thruster with magnetic nozzle,” *Physics of Plasmas*, Vol. 30, No. 2, 02 2023, pp. 023506.
- ⁴Peterschmitt, S., *Development of a Stable and Efficient Electron Cyclotron Resonance Thruster with Magnetic Nozzle*, Ph.D. thesis, Institut Polytechnique de Paris, 2022.
- ⁵Désangles, V. et al., “ECRA thruster advances, 30W and 200W prototypes latest performances,” *37th International Electric Propulsion Conference*, 2022.
- ⁶Meeker, D., “Finite Element Method Magnetics, Version 4.2,” <https://www.femm.info>, [28-Feb-2018 Build].
- ⁷Masillo, S. et al., “Validation of a torsional balance for thrust measurements of Hall effect and microwave-based space propulsion systems,” *Review of Scientific Instruments*, Vol. 93, No. 11, 11 2022, pp. 114501.
- ⁸Lobbia, R. B. and Beal, B. E., “Recommended Practice for Use of Langmuir Probes in Electric Propulsion Testing,” *Journal of Propulsion and Power*, Vol. 33, No. 3, 2017, pp. 566–581.
- ⁹Brown, D. L. et al., “Recommended Practice for Use of Faraday Probes in Electric Propulsion Testing,” *Journal of Propulsion and Power*, Vol. 33, No. 3, 2017, pp. 582–613.